Förster Resonance Energy Transfer Evidence for Lysozyme Oligomerization in Lipid Environment

Valeriya M. Trusova,*,† Galyna P. Gorbenko,† Pabak Sarkar,‡ Rafal Luchowski,‡,∥ Irina Akopova,‡ Leonid D. Patsenker,⊥ Oleksii Klochko,⊥ Anatoliy L. Tatarets,⊥ Yuliia O. Kudriavtseva,⊥ Ewald A. Terpetschnig,# Ignacy Gryczynski,‡,▽ and Zygmunt Gryczynski‡,§

Department of Biological and Medical Physics, V. N. Karazin Kharkov National University, 4 Svobody Sq., Kharkov 61077, Ukraine; Center for Commercialization of Fluorescence Technologies, Department of Molecular Biology and Immunology, University of North Texas Health Science Center, 3500 Camp Bowie Blvd., Fort Worth, Texas 76107, United States; Department of Physics, Texas Christian University, 2800 S. University Dr., Fort Worth, Texas 76129, United States; Department of Biophysics, Institute of Physics, Maria Curie-Sklodowska University, 20-031 Lublin, Poland; STC "Institute for Single Crystals" of the National Academy of Sciences of Ukraine, 60 Lenin Ave., Kharkov 61001, Ukraine; SETA BioMedicals, LLC, 2014 Silver Ct East, Urbana, Illinois 61801, United States; and Department of Cell Biology and Genetics, University of North Texas Health Science Center, 3500 Camp Bowie Blvd., Fort Worth, Texas 76107, United States

Received: September 20, 2010; Revised Manuscript Received: November 4, 2010

Intermolecular time-resolved and single-molecule Förster resonance energy transfer (FRET) have been applied to detect quantitatively the aggregation of polycationic protein lysozyme (Lz) in the presence of lipid vesicles composed of phosphatidylcholine (PC) and its mixture with 5, 10, 20, or 40 mol % of phosphatidylglycerol (PG) (PG5, PG10, PG20, or PG40, respectively). Upon binding to PC, PG5, or PG10 model membranes, Lz was found to retain its native monomeric conformation, while increasing content of anionic lipid up to 20 or 40 mol % resulted in the formation of Lz aggregates. The structural parameters of protein self-association (the degree of oligomerization, the distance between the monomers in protein assembly, and the fraction of donors present in oligomers) have been derived. The crucial role of the factors such as lateral density of the adsorbed protein and electrostatic and hydrophobic Lz−lipid interactions in controlling the protein self-association behavior has been proposed.

1. Introduction

Over the past decade, the phenomenon of protein self-assembly into supramolecular clusters attracts ever growing attention due to the recognition of intimate causative link between this process and etiology of several debilitating disorders such as Alzheimer's, Creutzfeld−Jacob's, Parkinson's, Huntington's diseases, systematic amyloidosis, type II diabetes, amyotrophic lateral sclerosis, etc.[1,2] Accumulating evidence from both theoretical and experimental studies suggests that protein aggregation requires the partial unfolding of the native state into aggregation-prone intermediate transient conformation with the exposed hydrophobic regions, intermolecular contacts between which are responsible for oligomerization.[3] The factors facilitating protein unfolding and subsequent aggregation were shown to involve milieu conditions (acidic pH, elevated temperature), the presence of organic solvents and denaturants, or protein adsorption onto phospholipid surfaces such as monolayers or bilayers.[4−6] The crucial role of lipid/water interfaces in initiating and regulating the polypeptide self-association consists not only in acting as passive template for protein aggregate formation and growth but also in providing unique physicochemical environment which favors (i) the recruitment of protein molecules increasing thereby their local concentration necessary for oligomer nucleation, (ii) attenuation of electrostatic repulsion between charged monomers, (iii) destabilization of protein native structure, resulting in formation of aberrant unfolded states of polypeptide chain, and (iv) peculiar alignment of protein molecules promoting the polymerization.[7,8] Given the dramatic impact of protein oligomers on the development of severe diseases, and allowing for the perceived importance of lipid matrices in polypeptide self-assembly, accurate detection and characterization of lipid-assisted protein aggregation are of utmost significance, since timely identification of oligomers may help to prevent their conversion into pathogenic species. To date, the vast majority of experimental techniques including circular dichroism,[9] atomic force and electron microscopy,[10,11] electron paramagnetic resonance,[12] etc. has been employed to clarify the role of lipid bilayer in protein aggregation. Although these techniques contribute significantly to the fundamental understanding of membrane-promoted self-association of polypeptides, the complex nature of this process requires the development of novel sophisticated but at the same time convenient approaches which can provide rapid detection as well as direct output of structural parameters of protein oligomerization at the lipid−water interface without perturbation

* Corresponding author. Address for correspondence: 19-32 Geroyev Truda St., Kharkov 61144, Ukraine. Tel.: +38 057 343 82 44, +38 0572 68-41-49. E-mail: valtrusova@yahoo.com.

† V. N. Karazin Kharkov National University.

‡ Department of Molecular Biology and Immunology, University of North Texas Health Science Center.

§ Texas Christian University.

∥ Maria Curie-Sklodowska University.

⊥ National Academy of Sciences of Ukraine.

SETA BioMedicals.

▽ Department of Cell Biology and Genetics, University of North Texas Health Science Center.

10.1021/jp108976e
Published on Web 12/02/2010

of the system under study. Förster resonance energy transfer (FRET) represents a significant breakthrough in the field of biomolecular interactions occurring at nanometer distances and constitutes an ideal analytical tool that fully satisfies all the above criteria. The uniqueness of this spectroscopic technique lies in elegant combination of distance-dependent manner of radiationless energy transfer between donor and acceptor dipoles with attractive advantages of fluorescence spectroscopy—high informativity, relative simplicity, noninvasive nature, potential for real time in vivo cellular applications, and experimental convenience. Successful application of FRET in monitoring the protein−protein interactions has been reported while exploring the aggregation of membrane-bound mellitin,[13,14] phospholamban,[15] calcium ATPase,[16] 5-HT1A receptor,[17] glycophorin A,[18] and β_2-adrenoceptor.[19]

In the present work, we applied the advanced FRET techniques, viz., time-resolved FRET (tr-FRET) and single-molecule pulse interleaved excitation FRET (PIE-FRET) to detect the self-association of polycationic protein lysozyme (Lz) in the lipid bilayers composed of phosphatidylcholine (PC) and its mixtures with phosphatidylglycerol (PG). The donor−acceptor pairs were represented by fluorescein 5′-isothiocyanate (Fl) and DyLight 549 (DyL_{549}) (tr-FRET studies) or Fl and SeTau-647-di-NHS (SeTau647) (PIE-FRET experiments), respectively, covalently attached to Lz. In our previous work, the utilization of different modifications of steady-state fluorescence spectroscopy provided the proofs for Lz oligomerization upon the binding to negatively charged lipid vesicles.[20] However, these studies represent an indirect detection of protein self-association that averages the fluorescence signal over all emitting species and does not resolve conformational or distance distribution of Lz monomers within the protein cluster. FRET approach, presented here, is anticipated to overcome these restrictions and yield more precise information on lysozyme self-association behavior in the presence of lipid membranes. More specifically, we concentrated our efforts on (i) quantitative detection of lipid-mediated Lz aggregates; (ii) calculation of the degree of oligomerization, n, the distance between the monomers in protein assembly, R_a, and fraction of donors present in oligomers, X; (iii) deciphering the impact of membrane charge and surface coverage with the adsorbed protein on the above parameters.

2. Materials and Methods

2.1. Materials. Chicken egg white lysozyme, fluorescein 5′-isothiocyanate (Fl), HEPES, and dithiothreitol (DTT) were purchased from Sigma (St. Louis, MO). 1-Palmitoyl-2-oleoyl-*sn*-glycero-3-phosphocholine (PC) and 1-palmitoyl-2-oleoyl-*sn*-glycero-3-phospho-*rac*-glycerol (PG) were from Avanti Polar Lipids (Alabaster, AL). Dimethyl sulfoxide was of Uvasol grade from Merck (Whitehouse Station, NJ). 1-Ethyl-3-[3-dimethylaminopropyl]carbodiimide hydrochloride (EDC), DyLight 549 (maleimide-activated form), and sodium borate buffer, pH 9, were provided by Thermo Fisher Scientific (Rockford, IL). Phosphate-buffered saline (PBS), pH 7.4, was from Amresco (Solon, OH). SeTau-647-di-NHS ($SeTau_{647}$) was provided by SETA BioMedicals (Urbana, IL).

2.2. Lysozyme Labeling with Fluorescent Labels. ***2.2.1. Protein Labeling with Fl.*** Reaction mixture containing equimolar amounts of Fl and Lz, was prepared in 100 mM borate buffer. After incubation of the sample for 90 min at 25 °C under continuous stirring in the dark, pH was adjusted to 7.4. Subsequently, the solution was dialyzed at 4 °C against 20 mM HEPES, pH 7.4. The degree of labeling was estimated using extinction coefficients of 7.3×10^4 M^{-1} cm^{-1} for Fl at 494 nm and 3.3×10^4 M^{-1} cm^{-1} at 280 nm for Lz. Protein concentration was calculated after subtracting Fl absorbance using extinction coefficient of 3.7×10^4 M^{-1} cm^{-1} at 280 nm, and revealed a fluorescein–protein molar ratio of 0.91.

2.2.2. Protein Labeling with DyLight 549. A 0.5 mg sample of Lz was dissolved in 0.5 mL of 20 mM HEPES, pH 7.4, and subsequently mixed with DTT to reduce protein disulfide bonds. DTT:Lz molar ratio was 10:1. Afterward, this mixture was incubated for 1.5 h at continuous stirring and dialyzed against 20 mM HEPES, pH 7.4 for 2 h. Reduced Lz solution was mixed with DyL_{549} prepared by dissolving 1 mg of the label in 1 mL of DMSO. This reaction mixture was incubated for 2 h at 37 °C in the dark and then centrifuged at 14 000g for 10 min to precipitate protein aggregates which may be present in solution. Afterward, the supernatant containing DyL_{549}-labeled Lz monomers and free label was dialyzed against 20 mM HEPES, pH 7.4, overnight to separate bound and unbound dye. Protein concentration and degree of labeling (D/P) were calculated spectrophometrically by measuring the absorbance of conjugate at 280 and 562 nm, using extinction coefficients 3.3×10^4 M^{-1} cm^{-1} at 280 nm and 1.5×10^5 M^{-1} cm^{-1} at 562 nm for Lz and DyL_{549}, respectively. Calculated in such a way, the protein concentration was found to be 75 μM and D/P was 0.35.

2.2.3. Protein Labeling with SeTau-647-di-NHS. Stock solution of Lz was made by dissolving 1 mg of the protein in 1 mL of borate buffer, pH 9. Before the preparation of the reaction mixture, functional groups of the label were additionally activated by dissolving 1 mg of $SeTau_{647}$ and 0.4 mg EDC in 1 mL of PBS, pH 7.4. Afterward, protein solution and activated label were mixed and incubated at continuous stirring for 6 h. After incubation, free and bound dyes were separated using Sephadex columns G25. To prevent $SeTau_{647}$ degradation, all solutions were wrapped in the foil and kept in the dark. Measuring the absorbance of conjugate at 280 and 650 nm, using extinction coefficients 3.3×10^4 M^{-1} cm^{-1} at 280 nm and 3.7×10^5 M^{-1} cm^{-1} at 650 nm for Lz and $SeTau_{647}$, respectively, yielded protein concentration and D/P of 15 μM and 0.15.

2.3. Preparation of Lipid Vesicles. Large unilamellar vesicles were made by extrusion technique from PC and its mixtures with 5, 10, 20, and 40 mol % PG.[21] Appropriate amounts of lipid stock solutions were mixed in chloroform, evaporated to dryness under a gentle nitrogen stream, and then left under reduced pressure for 1.5 h to remove any residual solvent. The dry lipid films were subsequently hydrated with 20 mM HEPES, pH 7.4 at room temperature to yield lipid concentration of 1 mM. Thereafter, the samples were subjected to 15 passes through a 100 nm pore size polycarbonate filter (Millipore, Bedford, MA), yielding the liposomes of desired composition. Hereafter, liposomes containing 5, 10, 20, and 40 mol % PG are referred to as PG5, PG10, PG20, and PG40, respectively.

2.4. Fluorescence Measurements. All measurements were performed at room temperature in 20 mM HEPES in 1 cm path length quartz cuvettes. Steady-state fluorescence experiments were done with Varian Cary Eclipse spectrofluorimeter (Varian Inc.). Fluorescein excitation wavelength was 490 nm. Excitation and emission slit widths were set at 5 nm. Fluorescence intensity measured in the presence of DyL_{549} at the maximum of Fl emission (517 nm) was corrected for reabsorption and inner filter effects using the following coefficient:

$$k = \frac{(1 - 10^{-A_o^{ex}})(A_o^{ex} + A_a^{ex})(1 - 10^{-A_o^{em}})(A_o^{em} + A_a^{em})}{(1 - 10^{-(A_o^{ex}+A_a^{ex})})A_o^{ex}(1 - 10^{-(A_o^{em}+A_a^{em})})A_o^{em}} \quad (1)$$

where A_o^{ex} and A_o^{em} are the donor optical densities at the excitation and emission wavelengths in the absence of acceptor, and A_a^{ex} and A_a^{em} are the acceptor optical densities at the excitation and emission wavelengths, respectively.

Time-resolved fluorescence measurements were carried out with a FluoTime200 fluorometer (PicoQuant GmbH) equipped with an ultrafast microchannel plate detector capable to well resolve subnanosecond decays. 470 nm pulsed laser diode LDH-PC-470 (PicoQuant GmbH) in the low-power regime (full width at half-maximum for the pulse was <70 ps) with 5 MHz repetition rates was used as excitation source. The laser diode is routinely used to measure fluorescence decays and lifetimes within ±10 ps accuracy. The lifetime data were analyzed by FluoTime software, version 4.0 (PicoQuant GmbH). For lifetime measurements, a monochromator supported by long wave pass filter on the observation path was used. All the measurements for lifetime decay were performed using magic angle conditions. The decay was fitted to a multiexponential model using the expression

$$I(t) = \sum_{i=1}^{n} \alpha_i e^{-t/\tau_i} \quad (2)$$

where $I(t)$ is the fluorescence intensity at time t and α_i and τ_i are respectively the amplitude and lifetime of ith component.

The mean lifetime $\langle\tau\rangle$ was calculated as

$$\langle\tau\rangle = \sum_{i=1}^{n} \alpha_i \tau_i^2 / \left(\sum \alpha_i \tau_i\right) \quad (3)$$

2.5. PIE-FRET Studies. Single-molecule experiments for pulse interleaved excitation (PIE) were carried on a MicroTime 200 confocal fluorescence microscope system (PicoQuant GmbH, Germany). The pulsed excitation laser beams (470 nm for donor and 635 nm for acceptor) were directed by dichroic mirror to a high numerical aperture (NA) water objective (60 × NA 1.2) and was focused 10 μm above the surface of the coverslip, into the sample volume. The collected fluorescence was split by a dichroic beam splitter (600DCXR, Chroma Technology) and spectrally filtered with emission bandpass filter 550/88 (Semrock) for donor and combination of long wavelength pass filters 647 and 650 (Semrock and Edmund Optics, respectively) for acceptor. The emission was collected simultaneously by two avalanche photodiodes (MPD, PDM 1CTC) and processed by the PicoHarp300 time-correlated single-photon-counting module. The lasers were each triggered with a repetition rate of 20 MHz and the 470 nm laser pulse was delayed by 25 ns with respect to the 635 nm laser. The integration time used to obtain donor−acceptor time trace was 5 min. The data was analyzed with SymPhoTime (version 5.0) software package that controlled the data acquisition as well. For the purpose of data analysis, two decay curves received for donor and acceptor emission were analyzed separately.[22] The energy transfer efficiency E could be calculated as described earlier according the formula[23]

$$E = \frac{F_{D_{ex}}^{A_{em}}}{F_{D_{ex}}^{A_{em}} + \gamma F_{D_{ex}}^{D_{em}}} \quad (4)$$

γ is a detection correction factor defined as

$$\gamma = \frac{\phi_D \eta_D}{\phi_A \eta_A} \quad (5)$$

where $F_{D_{ex}}^{A_{em}}$ is an emission intensity signal of the acceptor after donor excitation, $F_{D_{ex}}^{D_{em}}$ is an emission intensity signal of the donor with donor excitation, η_D and η_A are donor and acceptor detection efficiencies, and ϕ_D and ϕ_A are quantum yields of donor and acceptor, respectively. For our system with Fl working as a donor and SeTau647 as an acceptor, detection correction was equal to 0.8.

3. Theoretical Background

3.1. General Theory of FRET in Two Dimensions. In the absence of acceptors fluorescence decay of the donor is described by

$$I_D(t) = \exp(-t/\langle\tau_0\rangle) \quad (6)$$

In the case of randomly diffusing donor and acceptors, donor fluorescence decay can be written as

$$I_{DA}(t) = \exp(-t/\langle\tau\rangle - C(-t/\langle\tau\rangle)^{1/3}) \quad (7)$$

where

$$C = \Gamma\left(\frac{2}{3}\right) c_A^s \pi R_0^2 \quad (8)$$

Here, c_A^s is the acceptor surface concentration related to the mean area per lipid molecule (S_L) and molar concentrations of lipids accessible to acceptor ($0.5L$, L is the total lipid concentration) and bound acceptor (B_A) as $c_A^s = B_A/0.5LS_L$; Γ is the incomplete gamma function, R_0 is the Förster radius depending on donor quantum yield (Q_D) and the overlap between donor emission ($F_D(\lambda)$) and acceptor absorption ($\varepsilon_A(\lambda)$) spectra

$$R_0 = 979(\kappa^2 n_r^{-4} Q_D J)^{1/6}; \quad J = \frac{\int_0^\infty F_D(\lambda)\varepsilon_A(\lambda)\lambda^4 \, d\lambda}{\int_0^\infty F_D(\lambda) \, d\lambda} \quad (9)$$

where n_r is the refractive index of the medium ($n_r = 1.37$) and κ^2 is an orientation factor. Förster radius was found to be 5.63 nm for Fl−DyL_{549} donor−acceptor pair and 5.8 nm for Fl−$SeTau_{647}$ taking $\kappa^2 = 0.67$.[24]

Assuming that there is no homotransfer between the donors, and donor−acceptor exclusion radius is much smaller than R_0, C takes the value of $C \approx 4.254 c_A^s R_0^2$.[25] To estimate c_A^s, the concentration of bound acceptor was calculated within the framework of scaled particle theory-based adsorption models described in detail elsewhere.[20,26]

3.2. FRET in Protein Oligomers. FRET data in the oligomeric complex were analyzed according to the simulation

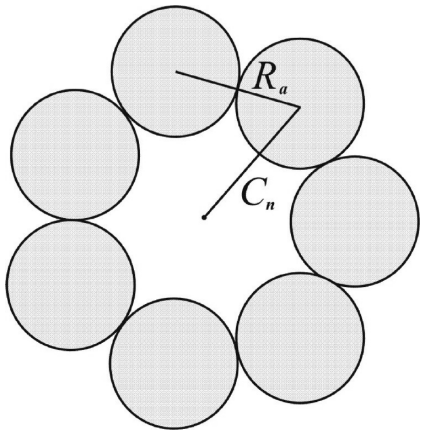

Figure 1. Schematic representation of the protein ring-shaped oligomer structure (adapted from ref 15).

procedure developed by Li et al.[15] Lz aggregates are modeled as symmetric ring-shaped structures consisting of n subunits (monomers) (Figure 1). All subunits (indexed by j) are assumed to be labeled with either donor or acceptor and mixed randomly. Protein oligomers are supposed to be in thermodynamic equilibrium with monomeric species. Energy transfer, calculated in terms of binomial distribution of the number of donors in oligomer, is given by

$$E = 1 - 1/[n(1 - P_A)]\sum_{i=1}^{n} i\binom{n}{i}P_A^{n-1}(1 - P_A)^i[1 - E_i(R_a)] \quad (10)$$

where P_A is the molar fraction of acceptor, calculated taking into account the degree of labeling, R_a is the distance between donor and acceptor on different subunits, and $E_i(R)$ is the averaged energy transfer intensity when the oligomer contains i donors.

The normalized fluorescence intensity of monomeric donor is given as $F(t)/F(0) = \exp(-k_D t)$, where k_D is donor decay rate in the absence of acceptor. For a dimer, the second subunit is assumed to be either an acceptor (with probability P_A) or donor (with probability $1 - P_A$) and so there will be two components in the decay, $(1 - P_A)\exp(-k_D t)$ and $P_A \exp[-(k_D + k_2)t]$, where k_2 is the rate constant for energy transfer to the acceptor at position 2. Each subsequent subunit will double the number of fluorescence decay components. Thus, for example for a trimer the normalized fluorescence decay can be written as

$$\frac{F(t)}{F(0)} = P_D P_D \exp(-k_D t) + P_A P_D \exp(-(k_D + k_2)t) + P_D P_A \exp(-(k_D + k_3)t) + P_A P_A \exp(-(k_D + k_2 + k_3)t) \quad (11)$$

For a given donor the resulting rate constant is a sum of rate constant contributed by each acceptor, so the exponential fluorescence decay terms are multiplied yielding the general expression for the time-resolved fluorescence intensity decay

$$I(t) = \exp(-k_D t)\prod_{j=2}^{n}[P_D X + P_A \exp(-k_j t)] \quad (12)$$

where P_D is the molar fraction of donor, X is the fraction of monomeric donors that take part in aggregation, and k_j is energy transfer rate from donor to acceptor on subunit j, determined as

$$k_j = k_D(r_j/R_0)^{-6} \quad (13)$$

Here r_j is the distance between donor and acceptor on subunit j

$$r_j = 2C_n \sin[\pi(j - 1)/n] \quad (14)$$

where $C_n = R_a/[2 \sin(\pi/n)]$ is apparent radius of protein oligomer.

Steady-state fluorescence intensity can be written as

$$F_{DA} = \int_0^\infty I(t)\,dt \quad (15)$$

and the corresponding transfer efficiency is given by

$$E = 1 - F_{DA}/F_D \quad (16)$$

where F_{DA} and F_D are donor steady-state fluorescence intensities in the presence and absence of acceptor, respectively.

Importantly, when FRET was measured by monitoring the changes in the averaged lifetimes of donor upon acceptor addition, the results were consistent with those obtained from steady-state measurements.

4. Results

At the first step of the study, intermolecular FRET from Fl to DyL_{549} covalently bound to Lz (Lz−Fl and Lz−DyL_{549}, respectively) has been employed for probing the formation of Lz oligomers. Equal amounts of donor (Lz−Fl) were incubated with the lipid vesicles of different compositions at four lipid concentrations (L = 25, 50, 75, or 100 μM), then titrated with the acceptor (Lz−DyL_{549}), and afterward the donor steady-state fluorescence intensity and fluorescence decay were recorded. Control experiments were performed in buffer solution without liposomes at the same concentrations of donor and acceptor. No FRET was detected in control and in the case when Lz−Fl was incorporated into PC or PG5 vesicles at all L and PG10 membranes at L = 75 and 100 μM. In contrast, noticeable energy transfer was observed in the presence of PG10 liposomes at lower L values (L = 25 and 50 μM) and PG20 or PG40 vesicles at all lipid concentrations employed here, where Lz−DyL_{549} addition led to (a) reduction of Lz−Fl steady-state emission, (b) appearance of the acceptor emission band in donor fluorescence spectra (Figure 2A), and (c) decrease in Lz−Fl lifetime calculated from intensity decays shown in Figure 2B. Furthermore, energy transfer was found to enhance with increasing PG molar fraction and decreasing lipid concentration. In analyzing these data, one should bear in mind that FRET can occur between either aggregated or nonaggregated species but adjacent donors and acceptors. To differentiate between these two cases, deconvoluted fluorescence intensities $I_D(t)$ and $I_{DA}(t)$ were calculated according to eqs 6 and 7. The function $\{\ln[I_D(t)/I_{DA}(t)]\}^3$ plotted in Figure 3 should yield a straight line if FRET arises from freely diffusing donors and acceptors and adopt the cubic form in the opposite case.[14,25] Indeed, as shown in Figure

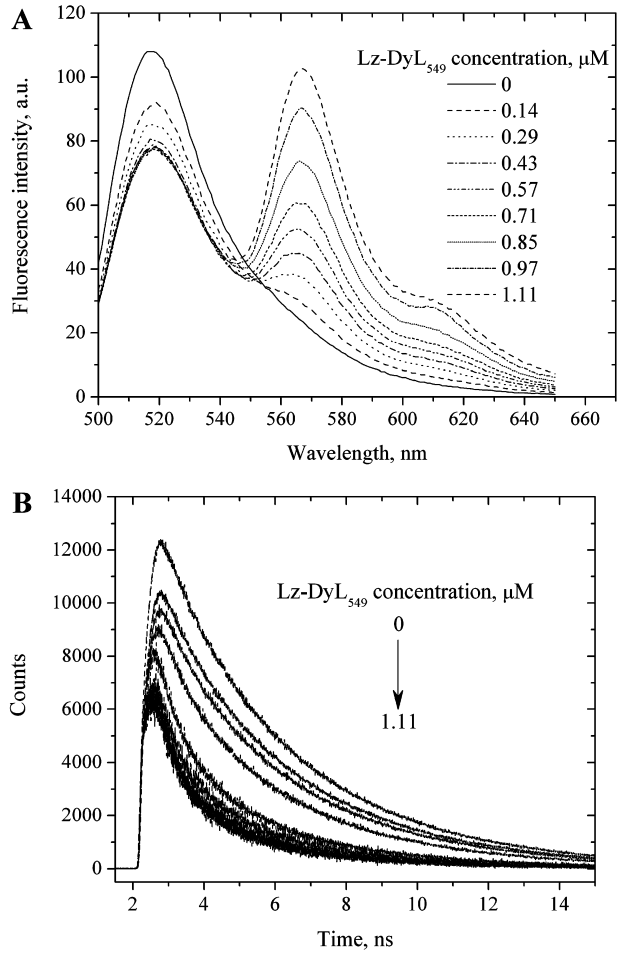

Figure 2. Steady-state fluorescence spectra (a) and time-resolved intensity decays (b) of donor Lz−Fl at varied concentration of acceptor Lz−DyL_{549} in PG20 liposomes. Lipid concentration was 25 μM.

3, the curves are linear for Lz bound to weakly charged PG10 bilayers and have parabolic shape for the protein incorporated into PG20 and PG40 membranes. This finding suggests that in the former case Lz retains its monomeric state, while in the latter one the observed FRET is between nonrandomly distributed, aggregated donors and acceptors. Next, PG20 and PG40 data were analyzed within the FRET model in protein oligomers (eqs 10−16) according to the following algorithm: (1) plotting the energy-transfer efficiencies (E) (Figure 4), obtained from steady-state measurements, vs the molar fraction of acceptor (P_A); (2) calculating the time-resolved fluorescence decays of Lz−Fl from eqs 12−14; (3) computing the donor steady-state fluorescence intensities (eq 15); (4) fitting the calculated curves (eq 16) to the experimental $E(P_A)$ dependencies by varying n, R_a, and X until the minimization of the error function, defined as $f = 1/(N)\sum_{i=1}^{N}(E_e - E_c)^2$, where N is the number of experimental data points and E_e and E_c are experimental and theoretical energy-transfer efficiencies, respectively. Further, to perform more accurate quantitative data processing, the range of possible R_a values was estimated using PIE-FRET technique. While traditional FRET may be polluted by zero efficiency populations due to non-FRET phenomena such as incomplete labeling, donor or acceptor photobleaching, etc., PIE-FRET enables the detection of true FRET events.[22,23] In brief, in the PIE-FRET the system is excited with two independent but synchronized laser pulses that have different wavelengths (in our case 470 and 630 nm). The laser pulses are delayed with respect to each other in order to produce the sequence of independent decays for donor and acceptor exited by each pulse separately. For short-wavelength excitation pulse both donor and acceptor are excited. The decay of the donor is easy to separate by a proper selection of filters (emission of the donor is in shorter wavelength typically corresponding to the absorption of acceptor). Long-wavelength pulse exclusively excites only acceptor, and only acceptor decay can be observed. In principle, the pulse separation should be much longer than the fluorescence lifetimes of donor and acceptor. In our case, the repetition rate of the laser system was 20 MHz and the delay between pulses 25 ns. In principle, the role of the second long-wavelength pulse is to detect if in the analyzed pair in a given moment of time an acceptor is present. During the analysis of acquired data, the software extracts and subsequently analyzes only those pairs where acceptor is present and the change in donor fluorescence lifetime is solely due to energy transfer to the acceptor. Partially inactive FRET pairs which cause interfering artifacts in standard FRET procedure are excluded. Figure 5 represents the histograms of FRET efficiency and donor−acceptor separation. As seen from the figure, two populations are observed: low-efficiency FRET fraction and medium-efficiency FRET fraction. Gaussian fit of FRET histograms revealed the peaks at ∼10% and ∼27% corresponding to low and medium efficiency FRET, respectively. The corresponding donor−acceptor separation distances were found to fall in the range from 4.2 to 7 nm with the peaks at ∼4.7 and ∼5.8 nm, respectively. The low FRET arises, probably, from energy transfer between nonadjacent monomer subunits, while energy transfer between neighboring subunits contributes to the higher efficiency fraction.

The estimates for donor−acceptor separation were taken as the upper and lower limits of R_a during the analysis of steady-state and time-resolved FRET results according to the above-mentioned algorithm. However, while trying to fit the results of FRET measurements with the described procedure, satisfactory agreement between theory and experiment ($f \leq 10^{-4}$) was achieved only at unrealistic degrees of oligomerization ($n \geq 25$). A question arises, what if the model parameters were incorrectly chosen? The main suspicion was on the orientation factor, the parameter whose uncertainty is regarded as the main source of errors, especially in calculation of Förster distance. Orientation factor ranges from 0 to 4, depending on the angle between donor emission and acceptor absorption transition dipoles and the angles between these dipoles and a vector joining the donor and acceptor.[24] In the case of perpendicular orientation of donor and acceptor dipoles, κ^2 is 0, while when dipoles are parallel, κ^2 is equal to 4. Due to the difficulties associated with exact estimation of orientation factor, it is generally assumed to be 0.67. This value describes the situation of isotropic and dynamic averaging conditions where donor and acceptor are freely rotating adopting any of the possible orientations during the donor excited-state lifetime.[24,27] Clearly, isotropic condition is not applicable for the case of highly anisotropic membrane environment where rotational mobilities of both donor and acceptor are restricted. Furthermore, it is evident that formation of interprotein contacts during aggregation, mediated by specific protein sites, impose severe restrictions on the donor and acceptor mobility, and isotropic condition is hardly satisfied. To overcome the problem of unknown orientation factor, in the following we allowed κ^2 to vary within its acceptable limits (from 0 to 4) to yield a more sensible determination of R_0 according to the following equation[24]

$$R_0 = R_0^{0.67}\sqrt[6]{\frac{\kappa^2}{0.67}} \qquad (17)$$

where $R_0^{0.67}$ is the Förster radius calculated at $\kappa^2 = 0.67$ ($R_0^{0.67} =$ 5.63 nm for Fl−DyL_{549} donor−acceptor pair, section 3.1). Sub-

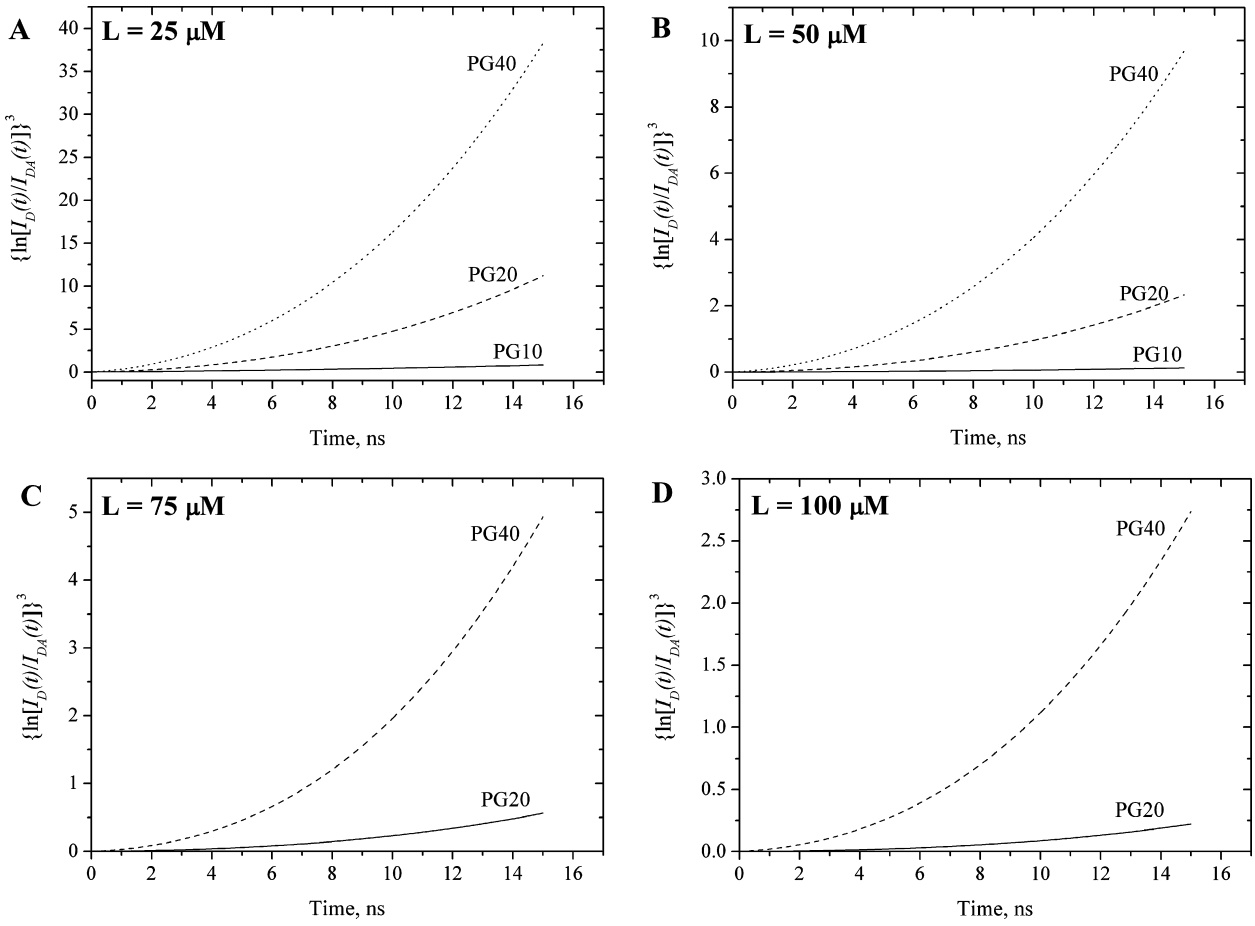

Figure 3. Cubic form of logarithmic function $\ln[I_D(t)/I_{DA}(t)]$ vs time for the different lipid concentrations. Lipid concentration was 25 (A), 50 (B), 75 (C), or 100 (D) μM.

stitution of this expression into eq 14 did significantly improve the fitting according to the algorithm steps 1−4, and allowed us to find the set of parameters (R_0, n, R_a, and X), which provides the best coincidence ($f \leq 9.8 \times 10^{-5}$) between theoretical and experimental curves (Figure 4). As shown in Table 1, increasing the content of anionic lipid PG resulted in the elevation of n and X, reduction of R_a reflecting the overall increase in Lz aggregation potential and tighter packing of monomers within the protein cluster. The same tendency was revealed at decreasing lipid concentration, or lipid/protein molar ratio, L/P.

In this context, it should be noted that the recovered estimates (Table 1) represent the only set of parameters ensuring the satisfactory agreement between the experimental and calculated data. In the model experiments, we varied the above parameters within the widest possible limits trying to find another set that would provide the adequate fit. However, as shown in representative plots in Figure 6, only the values of R_0, n, R_a, and X presented in Table 1 give the global minimum of f and ideal match between the experimental and simulated curves.

5. Discussion

The aggregation of protein molecules on the surfaces of biomembranes has been recognized to play a crucial role in signal transduction, immune response, development of neurological diseases, etc.[28−30] The paramount importance of protein oligomerization in controlling and regulating the normal cell functioning highlights the necessity of precise detection and correct enumeration of aggregated species on nanometer scale. Among a huge variety of analytical tools used for the quantification of polypeptide oligomerization, one of the leading positions belongs to FRET.[14−17,28] The characteristic nanometer distance scale of energy transfer phenomenon renders this technique particularly sensitive in quantitative analysis of protein clustering. Moreover, FRET can be considered not only as quantitative but also as qualitative method. Very often, the fact of presence or absence of FRET itself may be an indication of protein self-association.

In the present paper, FRET was utilized to monitor the impact of lipids on the aggregation state of lysozyme. Energy transfer was measured between fluorescent labels covalently attached to the protein.

5.1. Structure of Lz Oligomers Depends on Membrane Surface Electrostatic Potential and Lipid/Protein Molar Ratio. Comprehensive analysis of intermolecular FRET data revealed that Lz retains its native monomeric conformation in buffer or when bound to PC, PG5, and PG10 lipid vesicles. On the contrary, when PG content in the lipid bilayers reached 20 or 40 mol %, evidence for Lz transition into oligomeric state has been obtained with the effect being more pronounced at decreasing lipid concentration. In the most general case, enhancement of protein aggregation propensity in the presence of lipid membranes is attributed to the polypeptide conformational changes consistent with loosening of its tertiary structure and partial unfolding.[7] A growing body of evidence supports the idea that lipid bilayer lowers the activation energy barrier for protein unfolding providing an environment with reduced pH and decreased dielectric constant whose concerted action enhances side chain charge repulsion and thereby gives rise to a more open structure with the exposed aggregation-prone areas.

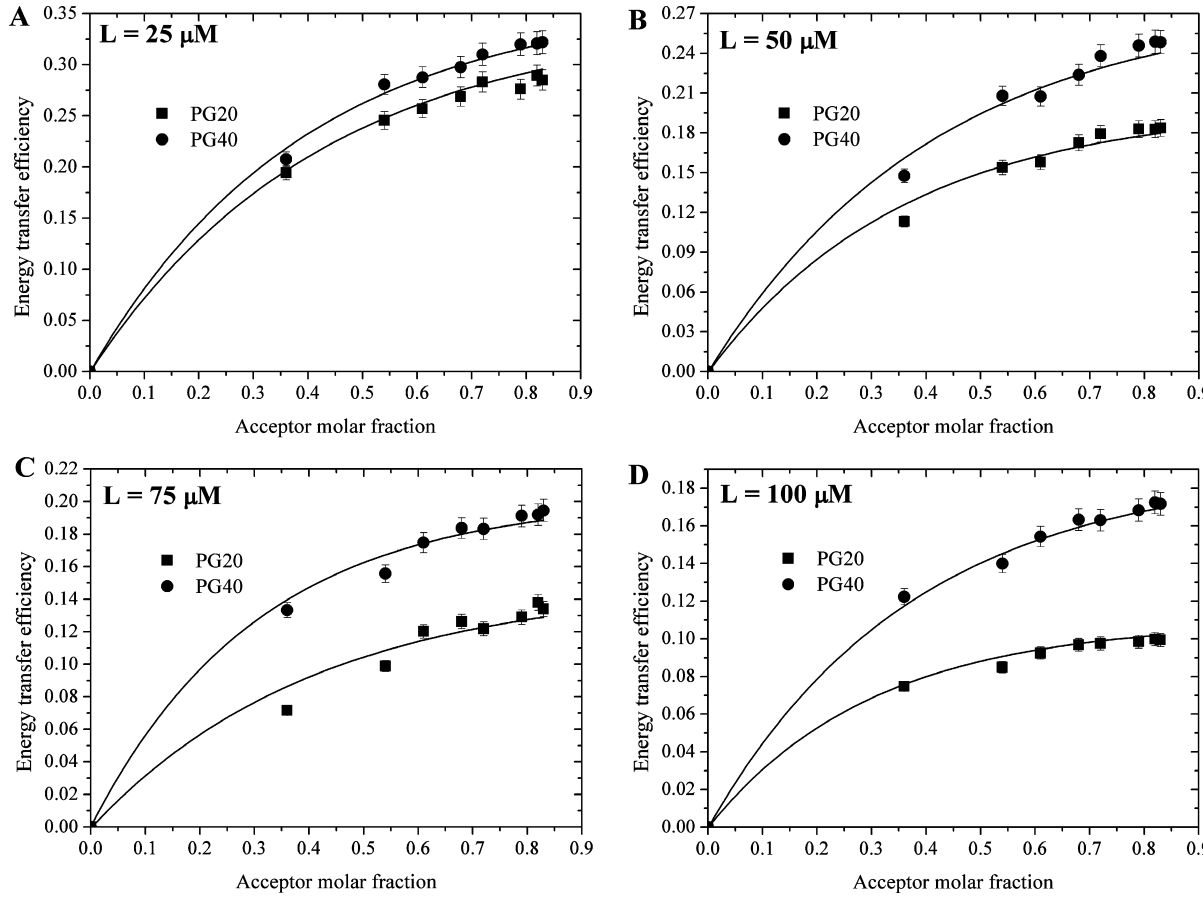

Figure 4. Energy-transfer efficiencies as a function of acceptor molar fraction. Solid lines represent theoretical curves providing the best fit. Lipid concentration was 25 (A), 50 (B), 75 (C), or 100 (D) μM.

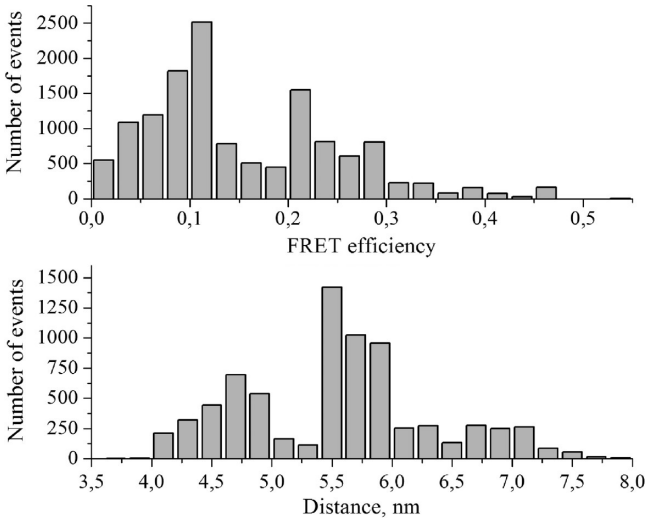

Figure 5. PIE-FRET histograms of distance and FRET efficiency distributions in PG40 lipid membranes. Lipid concentration was 50 μM. Donor−acceptor pair is represented by Lz−Fl and Lz−SeTau647.

Indeed, according to our estimates pH decrease compared to the bulk phase (pH 7.4) can be as large as 0.6, 1, 1.6, and 2.2 pH units for PG5, PG10, PG20, and PG40 vesicles, respectively. However, Lz is a very stable protein whose secondary and tertiary structures were shown to be virtually unperturbed even at pH = 0.6.[31] Furthermore, pH-controlled Lz oligomerization cannot rationalize the facilitation of attractive protein−protein interactions with increasing *L*. Thus, we concluded that reduced interfacial pH is unlikely to be the main determinant of protein aggregation in a membrane environment. Enhancing the electrostatic protein−lipid interactions followed by the screening of Lz charges by anionic lipid headgroups may represent an alternative driving force for increasing the oligomerization potential of Lz with PG fraction. However, this possibility is also in conflict with the observed impact of lipid concentration, or L/P ratio, on the characteristics of Lz aggregation. As was hypothesized by Oellerich et al. for the case of cytochrome *c*, at high L/P values, in excess of lipid, a lot of binding sites for the protein are available, and electrostatic association of the protein with the membrane surface seems to be predominant.[32] Lowering the L/P ratio weakens the electrostatic forces due to the neutralization of the protein and membrane charges because of the formation of protein−lipid complexes. As a result, protein insertion into the hydrophobic part of the membrane effectively competes with peripheral, electrostatically controlled protein binding. In other words, these considerations mean that if Lz aggregation in the presence of lipids is electrostatically driven, then *n* and *X* would increase with L/P. The revealed opposite tendency implies the electrostatic protein−lipid interactions not to be the sole factor triggering Lz conversion into aggregated state. Therefore, we should quest for the mechanism that could emerge the integral picture of lipid-assisted protein aggregation and provide satisfactory explanation for the (i) absence of Lz aggregation in buffer and PC, PG5, or PG10 membranes, (ii) facilitation of the protein−protein interactions upon rising PG content, and (iii) attenuation of Lz self-association at high *L*. In seeking such a mechanism, one should address a large group of theoretical studies unraveling the nature of membrane-mediated protein−protein interactions.[33−36] These studies suggest that the main pathway for protein self-association is the long-range membrane-mediated attraction between the bilayer inclu-

TABLE 1: Fitting Parameters for FRET Data in Lysozyme Oligomers

	PG20				PG40			
parameter	25 μM[a]	50 μM	75 μM	100 μM	25 μM	50 μM	75 μM	100 μM
R_0, nm	3.21	3.19	3.18	3.14	3.4	3.2	3.17	3.14
n	5.8	4.8	3.9	3.8	6.3	5.6	5.3	4.9
R_a, nm	6.3	6.35	6.31	6.26	6.23	6.3	6.12	6.13
X	0.52	0.44	0.35	0.33	0.65	0.54	0.48	0.4
$f \times 10^{-5}$	8.5	9.3	1.8	3.3	1.32	9.8	1.7	7.1

[a] The quantities presented in this column denote the lipid concentration.

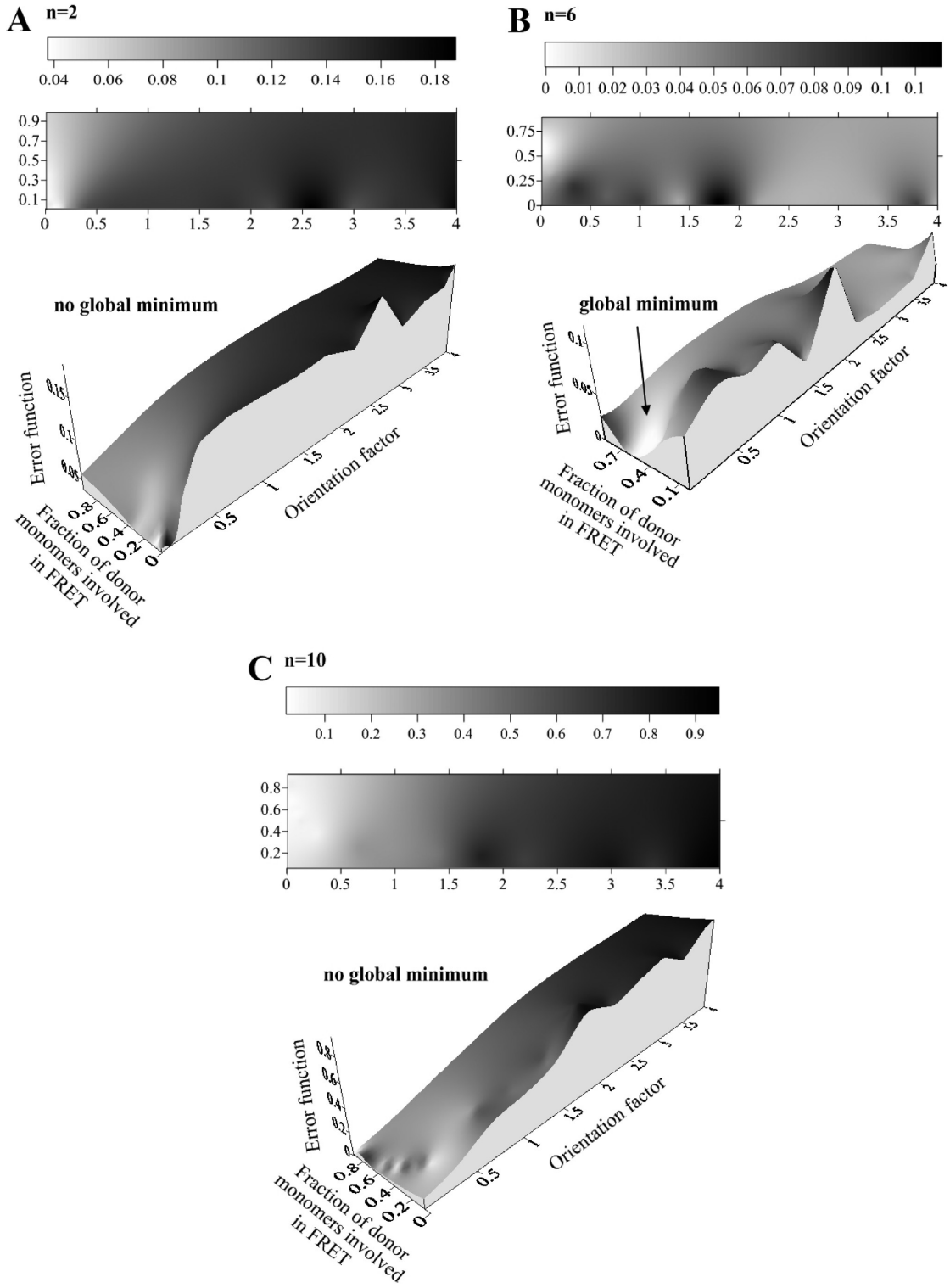

Figure 6. Error plots for FRET data in PG40 liposomes for the cases of Lz dimer (A), hexamer (B), and decamer (C).

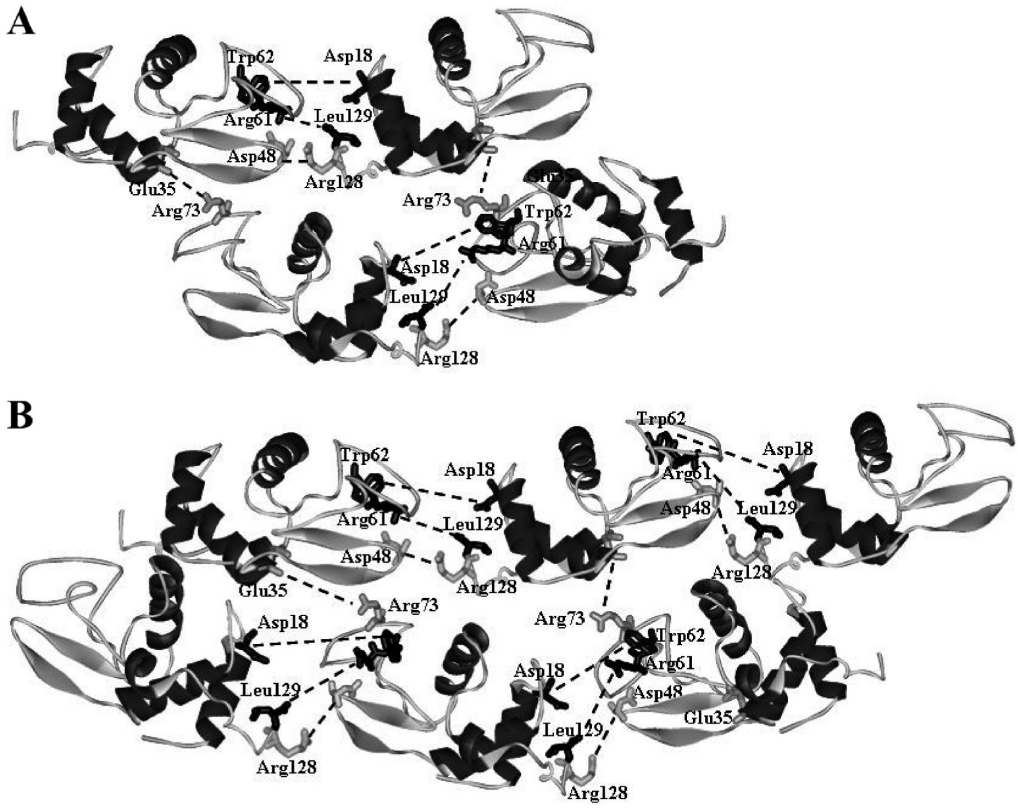

Figure 7. Tentative structures of Lz tetramer (A) and hexamer (B).

sions (proteins) arising from the overlap of membrane perturbations imposed by two neighboring inclusions. Speaking in more detail, when perturbed lipid annuli around the neighboring protein monomers overlap, attractive protein−protein interactions become energetically favorable, tending to minimize the overall free energy of protein-induced lipid bilayer deformations. Membrane deformations may include electrostatically controlled lipid demixing, implying the accumulation of oppositely charged lipids within the protein−membrane interaction zone, or elastic bilayer perturbations caused by hydrophobic mismatch principle and/or the changes in lipid order parameter, bilayer thickness, and area per lipid molecule.[35,37] These perturbations create the gradient of bilayer parameters across the boundary of the protein adsorption site and produce the positive line energy proportional to the circumference length of the protein−lipid interaction zone favoring the attractive interactions between the proteins because the circumference of two adjoining molecules is smaller than that of two isolated ones.[37]

Based on statistical mechanical theories, Lagüe et al. calculated that overlap of the perturbed lipid annuli is effective at the distances between protein monomers not exceeding 15 Å.[38] Such close proximity is possible at relatively high lateral densities of the adsorbed protein. If this is the case for our systems, then decreasing lipid concentration (at constant protein concentration) would raise the coverage of membrane surface by Lz molecules and enable the distorted lipid annuli around the adsorbed monomers to overlap, leading subsequently to the observed enhancement of Lz aggregation potential. The strengthening of self-association ability at increasing PG content can be explained in a similar manner. Evidently, Lz binding to neutral and PG5 or PG10 lipid vesicles is too weak to provide the protein lateral density necessary for overlap of lipid annuli. Elevation of anionic lipid fraction increases the concentration of bound protein and, consequently, its lateral density thereby decreasing the distance between the adsorbed monomers and ensuring the juxtaposing of perturbed lipid annuli.

The proposed scenario highlights the importance of membrane surface coverage with protein in governing the aggregation process and implies that lipid bilayer does not act as passive matrix in which protein clusters are formed but represents an active participant of polypeptide self-association.

5.2. Tentative Structure of Lz Aggregates. The reaction of Lz self-association has been thoroughly examined by a variety of techniques,[39−41] and a key role of electrostatic interactions in the formation of protein−protein complex has been demonstrated. Analysis of Lz dimerization reaction within the framework of encounter-complex formation theory allowed to identify two types of energetically favorable Lz complexes.[42] The first one involves the interactions between the following pairs of amino acid residues: $Lys_{33}-Asp_{48}$, $Arg_{112}-Glu_{35}$, $Glu_{35}-Arg_{73}$, and $Arg_{73}-Asp_{101}$. The electrostatic interaction energy of complex formation is −4.75 kcal/mol and the contact area is 224 Å^2. Complex of type II is stabilized by $Arg_{148}-Asp_{48}$ and $Leu_{129}-Arg_{61}$ contacts. The electrostatic interaction energy and contact area for this type of complex correspond to −6.3 kcal/mol and 84 Å^2, respectively. According to these findings, the structure of Lz tetra- or hexamer (the most frequent protein complexes in our systems, Table 1) may be tentatively depicted as shown in Figure 7.

In the present context, it is tempting to analyze how the proposed structure of Lz oligomers correlates with the derived values of intersubunit distance which actually represents the distance between fluorescent labels constituting the FRET pairs. Covalent attachment of Fl to protein molecule occurs in the amino groups of Lys residues while for DyL_{549} the target is SH groups of Cys residues. Lz contains six lysines and eight cysteines. Theoretically, each of these Lys and Cys residues may represent the potential site for covalent tagging with Fl or

DyL_{549}. However, lysozyme lysine residues have been reported to differ in their chemical properties.[43] Specifically, mass-spectrometric peptide-mapping analysis showed that the highest chemical reactivity is displayed by Lys_{33} and Lys_{97}. Therefore, we supposed that Fl tends to attach mainly to these Lz amino acid residues. The determination of the most probable site for DyL_{549} attachment is complicated by unknown distribution of chemical reactivities of lysozyme cysteines, so the identification of the most probable candidates for fluorescent labeling with DyL_{549} is hardly probable. However, we roughly calculated the distances between all possible donor−acceptor pairs that can be formed by the above Lys residues and all cysteines in two neighboring subunits of Lz oligomer, and the average distance was found to be ca. 6 nm, the value being in quite a good agreement with those given in Table 1.

6. Concluding Remarks

Overall, the results of the present study provide strong arguments in favor of lysozyme self-association in a membrane environment. The polypeptide transition from monomeric into oligomeric state is controlled by lateral density of the adsorbed protein and delicate balance of electrostatic and hydrophobic protein−lipid interactions. These findings are of utmost importance in the context of lysozyme amyloidogenesis, since detection of protein monomer self-association into critical oligomeric nucleus and identification of the inhibitors of this process represent the necessary prerequisite for the prevention of the amyloid-related disorders and creation of novel methods of their diagnostics and treatment.

Acknowledgment. This work was supported by grant No. 4534 from the Science and Technology Center in Ukraine, grant No. F28.4/007 from the Fundamental Research State Fund, grant NIH EB012334 (to Z.G.), and grant from European Social Fund (project no. 2009/0205/1DP/1.1.1.2.0/09/APIA/VIAA/152). V.T. gratefully acknowledges an award by the Human Frontier Science Program.

References and Notes

(1) Dobson, C. M. *Philos. Trans. Soc. London Ser. B* **2001**, *356*, 133–145.
(2) Selkoe, D. J. *Nature* **2003**, *426*, 900–904.
(3) Fink, A. L. *Folding Des.* **1998**, *3*, R9–R23.
(4) Zerovnik, E. *Eur. J. Biochem.* **2002**, *269*, 3362–3371.
(5) Aisenbrey, C.; Borowik, T.; Byström, R.; Bokvist, M.; Lindström, F.; Misiak, H.; Sani, M.; Gröbner, G. *Eur. Biophys. J.* **2008**, *37*, 247–255.
(6) McLaurin, J.; Yang, D. S.; Yip, C. M.; Fraser, P. E. *J. Struct. Biol.* **2000**, *100*, 259–270.
(7) Gorbenko, G. P.; Kinnunen, P. K. J. *Chem. Phys. Lipids* **2006**, *141*, 72–82.
(8) Relini, A.; Cavalleri, O.; Rolandi, R.; Gliozzi, A. *Chem. Phys. Lipids* **2009**, *158*, 1–9.
(9) Lau, T. L.; Ambroggio, E. E.; Tew, D. J.; Cappai, R.; Masters, C. L.; Fidelio, G. D.; Barnham, K. J.; Separovic, F. *J. Mol. Biol.* **2006**, *356*, 759–770.
(10) Widenbrant, M. J. O.; Rajadas, J.; Sutardja, C.; Fuller, G. G. *Biophys. J.* **2006**, *91*, 4071–4080.
(11) Wang, S. S.; Liu, K. N.; Lu, Y. C. *Biochem. Biophys. Res. Commun.* **2009**, *381*, 639–642.
(12) Hebda, J. A.; Miranker, A. D. *Annu. Rev. Biophys.* **2009**, *38*, 125–152.
(13) Hermetter, A.; Lakowicz, J. R. *J. Biol. Chem.* **1986**, *261*, 8243–8248.
(14) John, E.; Jähnig, F. *Biophys. J.* **1991**, *60*, 319–328.
(15) Li, M.; Reddy, L. G.; Bennett, R.; Silva, N. D.; Larry, J.; Jones, R.; Thomas, D. D. *Biophys. J.* **1999**, *76*, 2587–2599.
(16) Fagan, M. H.; Dewey, T. G. *J. Biol. Chem.* **1986**, *261*, 3651–3660.
(17) Woehler, A.; Wlodarczyk, J.; Ponimaskin, E. G. *Glycoconj. J.* **2009**, *26*, 749–756.
(18) Adair, B. D.; Engelman, D. M. *Biochemistry* **1994**, *33*, 5539–5544.
(19) Fung, J. J.; Deup, X.; Pardo, L.; Yao, X. J.; Velez-Ruiz, G. L.; DeVree, B. T.; Sunahara, R. K.; Kobilka, B. K. *EMBO J.* **2009**, *28*, 3315–3328.
(20) Gorbenko, G. P.; Ioffe, V. M.; Kinnunen, P. K. J. *Biophys. J.* **2007**, *93*, 140–153.
(21) Mui, B.; Chow, L.; Hope, M. *Methods Enzymol.* **2003**, *367*, 3–14.
(22) Kapanidis, A. N.; Lee, N. K.; Laurence, T. A.; Doose, S.; Margeat, E.; Weiss, A. *Proc. Natl. Acad. Sci. U.S.A.* **2004**, *101*, 8936–8941.
(23) Lee, N. K.; Kapanidis, A. N.; Wang, Y.; Michalet, Y.; Mukhopadhyay, J.; Ebright, R. H.; Weiss, S. *Biophys. J.* **2005**, *88*, 2939–2953.
(24) Lakowicz, J. R. *Principles of fluorescent spectroscopy*: Springer: New York, 2006.
(25) Wolber, P. K.; Hudson, B. C. *Biophys. J.* **1979**, *28*, 197–210.
(26) Chatelier, R.; Minton, A. P. *Biophys. J.* **1996**, *71*, 2367–2374.
(27) Dale, R.; Eisinger, J.; Blumberg, W. *Biophys. J.* **1979**, *26*, 161–194.
(28) Yeow, E. K. L.; Clayton, H. A. *Biophys. J.* **2007**, *92*, 3098–3104.
(29) Auer, S.; Dobson, C. M.; Venruscolo, M. *HFSP J.* **2007**, *1*, 137–146.
(30) Kumar, S.; Udgaonkar, J. B. *Curr. Sci.* **2010**, *98*, 639–656.
(31) Polverino de Laureto, P.; Frare, E.; Gottardo, R.; Van Dael, H.; Fontana, A. *Protein Sci.* **2002**, *11*, 2932–2946.
(32) Oellerich, S.; Lecomte, S.; Paternostre, M.; Heimburg, T.; Hildebrandt, P. *J. Phys. Chem.* **2004**, *108*, 3871–3878.
(33) Lagüe, P.; Zuckermann, M. J.; Roux, B. *Biophys. J.* **2000**, *79*, 2867–2879.
(34) Lagüe, P.; Zuckermann, M. J.; Roux, B. *Biophys. J.* **2001**, *81*, 276–284.
(35) Zemel, A.; Ben-Shaul, A.; May, S. *Biophys. J.* **2004**, *86*, 3607–3619.
(36) Harroun, T. A.; Heller, W. T.; Weiss, T. M.; Yang, L.; Huang, H. W. *Biophys. J.* **1999**, *76*, 937–945.
(37) Denisov, G.; Wanaski, S.; Luan, P.; Glaser, M.; McLaughlin, S. *Biophys. J.* **1998**, *74*, 731–744.
(38) Lagüe, P.; Zuckermann, M. J.; Roux, B. *Faraday Discuss.* **1998**, *111*, 165–172.
(39) Yonezawa, Y.; Tanaka, S.; Kubota, T.; Wakabayashi, K.; Yutani, K.; Fujiwara, S. *J. Mol. Biol.* **2002**, *323*, 237–251.
(40) Price, W. S.; Tsuchiya, F.; Arata, Y. *Biophys. J.* **2001**, *80*, 1585–1590.
(41) Gottshalk, M.; Halle, B. *J. Phys. Chem. B* **2003**, *107*, 7914–7922.
(42) Ermakova, E. *J. Mol. Model.* **2005**, *12*, 34–41.
(43) Suckau, D.; Mak, M.; Przybylski, M. *Proc. Natl. Acad. Sci. U.S.A.* **1992**, *89*, 5630–5634.

JP108976E